3-D Thermal and Seismic Structure of Slab and Plate Interface in Northern Cascadia

July 2005 Final Report: USGS Award Number: 03HQGR0102

K. Wang, G.C. Rogers, H. Dragert
Pacific Geoscience Centre, Geological Survey of Canada
9860 W Saanich Rd, Sidney, B. C., Canada V8L 4B2

Phone: (250)363-6429; Fax: (250)363-6565; Email: Kwang@nrcan.gc.ca

URL: http://www.pgc.nrcan.gc.ca

Element Designation: I and II, Pacific Northwest

Key Words: Thermophysical modeling, Seismotectonics, Wave propagation, GPS-continuous

Abstract. This project is designed to investigate what controls the damaging earthquakes within the subducting Juan de Fuca plate beneath the Pacific Northwest. Thermally controlled metamorphic processes as well as tectonic stresses are considered responsible for the generation of these earthquakes. To have a better understanding of the thermo-petrological process, we developed tomography models to constrain the rock properties in and around the slab and numerical models to understand the thermal field. We also compared the thermal and stress fields with the similar Nankai subduction zone in SW Japan, addressing the mechanics of earthquakes in warm slabs. The results provide (1) 3-D seismic tomography for northern Cascadia using earthquake and controlled-source data, (2) 2-D and 3-D modeling of mantle wedge flow and slab thermal structure for northern Cascadia.

1. Tomography

The tomography work was carried out by post-doctoral fellow Dr. Ramachandran using a method based on iterative linearized inversion of travel-time equations, with regularization by minimizing the vertical and horizontal roughness of the model subject to the constraint of fitting the travel-time data to within estimated observational uncertainties using the χ^2 criterion. Details of the method can be found in *Ramachandran et al.* [2005a]. The following text is mostly from a submitted paper by *Ramachandran et al.* [2005b].

1.1. Data

Data from an active source experiment and earthquake recordings were used to construct a 3-D *P*-wave minimum structure velocity model. The active source data constrains the upper crustal velocities that have large lateral variations between the sedimentary basins and the basement rocks made up of accreted terranes. The well-constrained upper crustal velocity structure improves the estimation of deeper velocities and earthquake hypocentral parameters.

The 1998 Seismic Hazards Investigation in Puget Sound (SHIPS) experiment [*Fisher et al.*, 1999; *Brocher et al.*, 1999] recorded arrivals from a total of 33,000 air-gun shots fired on 11 shot lines in the waterways of the Strait of Georgia, the Strait of Juan de Fuca, and Puget Sound (Figure 1). The shots were recorded widely over southwestern British Columbia and northwestern Washington at 257 temporary land-based Reftek stations, and 15 ocean-bottom seismometers at offsets from 1 to 370 km [*Brocher et al.*, 1999]. Approximately 147,000 first arrival times from 225 temporary recording stations were used in the inversion. In addition, 1000 first arrival travel times from a refraction line acquired in 1991 [*Miller et al.*, 1997] were included.

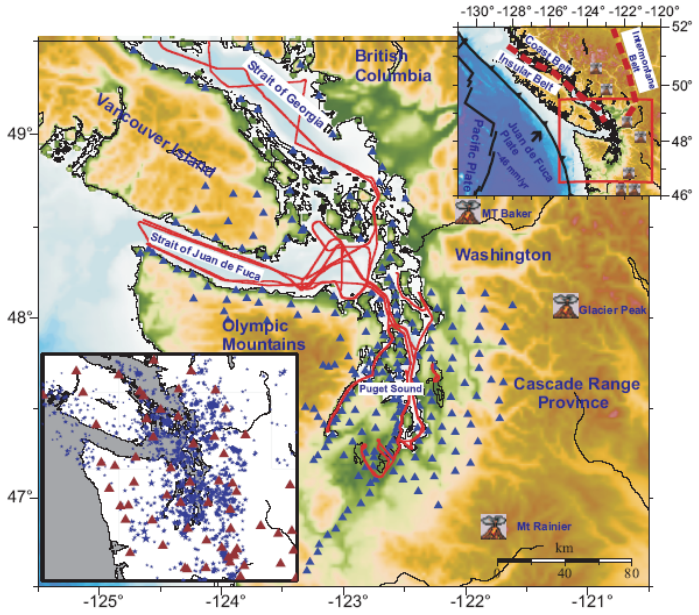

Figure 1. Location map showing the SHIPS temporary land based receiving stations (blue triangles) and air-gun shot positions (red lines) of the active source data used in the present study. Bottom left inset shows the earthquakes (blue stars) and permanent recording stations (red triangles) used in this study. Inset to the right top shows the plate tectonic regime of the study area.

Approximately 70,000 first arrival times from nearly 3000 earthquakes that occurred in the S.W. British Columbia and N.W.Washington margin, recorded at 91 permanent recording stations (Figure 1, left bottom inset) in the past 25 years were used in the tomographic inversion. Selection criteria included earthquakes from all depths, and recorded by at least six stations within the study region. The depth of the earthquakes ranged from 1 to 90 km and the magnitudes were above 1.0 and 2.0 for the British Columbia and Washington margins, respectively. Hypocentral parameters from the earthquake catalog were used as the initial hypocentral parameters for the inversion.

1.2. Velocity structure of the forearc upper mantle and slab

P-wave velocity models from the 3-D inversion are shown along six profiles (Figure 2) in Figures 3 and 4 with relocated earthquake hypocenters. In previous seismic studies, the forearc Moho is not observed beneath northern Cascadia margin and no sharp *PmP* reflections from the forearc Moho are reported [e.g., *Brocher et al.*, 2003]. Velocities of ~8.2 km/s are characteristic of cool uppermost mantle [e.g., *Mooney and Meissner*, 1995]. A moderate positive velocity gradient signature with a velocity increase from ~6.8 km/s to ~7.4 km/s probably marks the transition from forearc continental crust to forearc upper-mantle. The small velocity increase and the absence of a sharp velocity contrast at the boundary between the forearc crust and mantle can explain why *PmP* reflections are

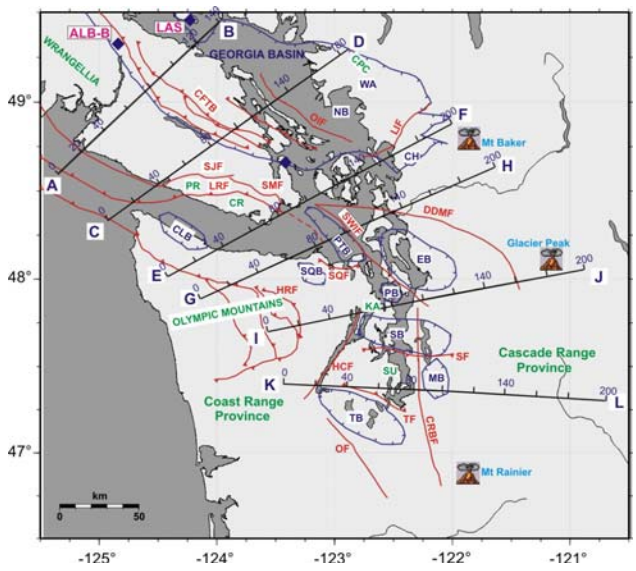

Figure 2. Locations of cross sections shown in Figures 3 and 4. The map also shows sedimentary basin (blue outlines) and geological faults (red lines) map.

absent in wide-angle recordings. The transition from lower crust to upper mantle is identified by a velocity increase from ~6.8 km/s to ~7.4 km/s at 35–40 km depth in profile AB (Figure 3a, model distance 90–130 km) and profile CD (Figure 3b, model distance 130-180 km). Close to these locations, *Cassidy and Ellis* [1993] estimated a depth of 36 km to the forearc mantle from a receiver function analysis. The low velocities of 7.4–7.8 km/s imaged at the above locations in profile AB and CD are in agreement with the forearc upper mantle velocity determined from previous refraction studies in this region.

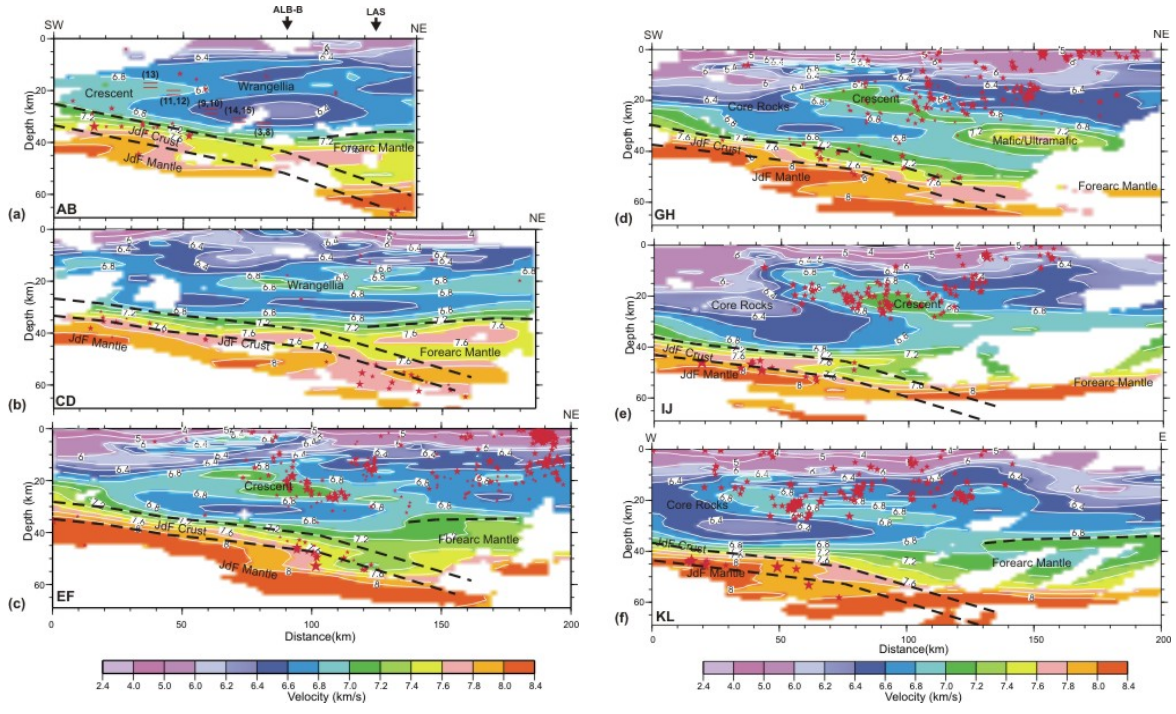

Figure 3. Cross-section view of P-wave velocities determined from tomographic inversion. Profile locations are shown in Figure 3. Red stars are earthquake hypocenters.

The velocity contrast between the lower continental crust and the Juan de Fuca crust is expected to be small and difficult to resolve from the smooth minimum structure velocity model. Howeve, the contrast between the oceanic crust (~6.8 km/s) and the oceanic mantle (~8.0 km/s) should be well resolved from the velocity model. In the smooth velocity model constructed in this study, the Juan de Fuca crust/mantle interface is defined by an intermediate velocity of ~7.6 km/s. The top of the oceanic crust is about 7 km higher, assuming an average oceanic crustal thickness.

1.3. In-slab earthquakes

It is previously suggested that oceanic slab earthquakes at depths below ~35 km are induced by the dehydration-embrittlement processes in the slab crust [e.g., *Kirby et al.*, 1996] and the deepest are induced as a result of the de-serpentinization dehydration reactions in the slab mantle [e.g., *Hacker et al.*, 2003]. On the vertical cross-sections (Figures 3 and 4), the earthquakes inferred to occur in the slab mantle lie in a region of velocity ranging from 7.6–8.0 km/s. From relocated slab earthquake positions beneath Strait of Georgia, *Cassidy and Waldhauser* [2003] demonstrated that some of the slab earthquakes originated from the oceanic mantle. Beneath Olympic Peninsula and Puget Sound, significant number of in-slab earthquakes lie in regions with velocities between 7.6 and 8.0 km/s. Almost fully eclogitized slab crust and partially serpentinized upper mantle are expected to be in this velocity range.

Seawater may percolate through fault zones on the subducting oceanic plate prior to subduction and could eventually hydrate and serpentinize the slab upper mantle. This process may reduce the velocity of the oceanic mantle to values below the normal ~8.2 km/s. Velocities in the range of 7.8–8.0 km/s at the inferred position of the slab mantle on the cross-sections in the Olympic Peninsula are possibly due to serpentinized peridotites in the slab mantle. As observed on the horizontal slice at 45 and 51 km depth, seismicity inferred in the slab mantle beneath the Washington margin is higher than the British Columbia margin. This can be explained by increased amounts of fluids released by oceanic mantle de-serpentinization below the Washington margin that facilitate seismic rupture.

The in-slab earthquakes are classified into three different groups: 6.8–7.2 km/s (slab upper crust with hydrous minerals), 7.2–7.8 km/s (mid to lower slab crust and partially eclogitized slab upper crust and serpentinized upper mantle), and 7.8–8.2 km/s (slab mantle that may be partially serpentinized).

The crust and uppermost mantle of warm slabs dehydrate at shallow depths [e.g., *Hacker et al.,* 2003; *Peacock and Wang*, 1999]. Thermal modeling for warm slabs like Juan de Fuca show that metamorphic reactions in the subducting oceanic crust can start at 40–50 km depth [*Peacock et al.*, 2002]. Depending on the amount of slab mantle serpentinization, earthquakes occurring in the slab mantle are expected to have a velocity of 7.8–8.2 km/s at the hypocenter. In contrast the earthquakes in the slab crust is expected to be in a region with 6.8–7.2 km/s range. Between 35–40 km depths, the number of earthquakes in the 6.8–7.2 km range is less than the number in the 7.2–7.8 km/s range. This suggests that more earthquakes occur in the slab's partially eclogitized upper crust having higher velocity range. The earthquakes in the 7.8–8.2 km/s are expected to be in the slab's nearly fully eclogitized crust and/or de-serpentinizing slab mantle. Between 40 and 50 km depths, a significantly larger number of earthquakes occur in the velocity

range of 7.8–8.0 km. This is indicative of earthquakes occurring close to the slab Moho. In this depth interval, fewer earthquakes are observed to occur in the velocity range of 6.8–7.2 km/s suggesting that the phase transformation reactions have altered the slab crust in this depth interval. At 50–60 km depth interval, the number of earthquakes in the 7.8–8.2 km/s interval dominate the distribution, and below 60 km depth no earthquakes are observed in the velocity range of 6.8–7.8 km/s. Hence, it is inferred that the earthquakes in the slab between 50 and 60 km depths occur in the nearly fully eclogitized crust and/or the upper mantle.

The above results suggest that a significant number of inslab earthquakes originate close to the slab Moho. *Wada et al.* [2004] showed that many events along the Nankai margin, SW Japan occur in the slab mantle. The recent warm-slab damaging earthquakes in the Cocos plate (Oaxaca, 1999, **M**7.5), the Philippine Sea plate (Geiyo, 2001,**M**6.7) and the Juan de Fuca plate (Nisqually, 2001, **M** 6.8) are inferred to have occurred close to the slab Moho [e.g., *Wang et al.*, 2004a]. Our results show that nine Cascadia in-slab earthquakes of **M >** 4 have a hypocentral velocity of 7.8–8.1 km/s, located between 40 and 55 km depth. The velocity at the hypocenter of these earthquakes indicate that they originate in the nearly fully eclogitized crust and/or close to the subducting slab Moho. This observation is consistent with the slab depth contours of McCrory et al. [2004].

Wang et al. [2004a] proposed that there is a tendency for large in-slab earthquakes to occur deep inside the slab. They argued that crustal densification in the upper few hundred meters of the slab crust will shatter and many earthquakes of smaller magnitudes may occur with small propagation distance. In addition they proposed that dehydration along hydrated existing faults in the slab's lower crust and upper mantle can facilitate seismic rupture that can propagate to large distances, resulting in large earthquakes. The postulation of *Wang et al.* [2004a] is consistent with the inference made in the present study that large inslab earthquakes in the Juan de Fuca plate occur close to the slab Moho. The damaging Geiyo, 2001 earthquake (**M** 6.7) in the Philippine Sea Plate occurred in the dehydrating region of slab crust and topmost slab mantle [*Wang et al.*, 2004b]. Large earthquakes occurring closer to the slab Moho, due to deserpentinization of the slab mantle and dehydration of the lower unaltered slab crust are probably not limited in size by the thickness of the slab crust. The faulting could extend from the slab crust into the slab upper mantle with larger propagation distance.

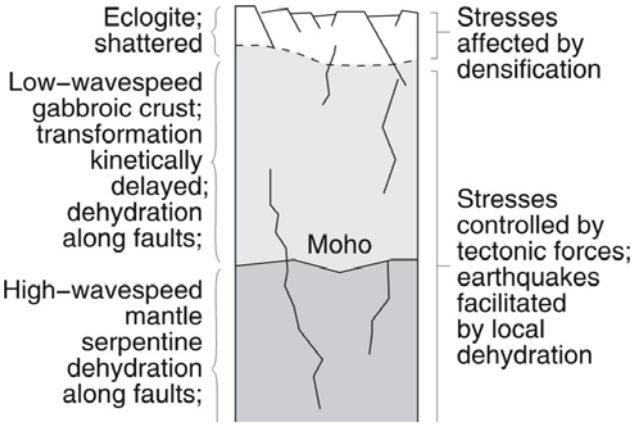

Figure 4. Metamorphic dehydration state of a warm slab slab in the 30-60 km depth range. The untransformed lower crust and mantle have a similar state of stress. From Wang et al. (2004a).

2. Thermal modeling

Thermal models provide information on the metamorphic conditions for the subducting slab and how slab dehydration may facilitate in-slab earthquakes. Two important constraints for regional-scale subduction zone thermal models are (1) a temperature as high as 1200-1300ºC in the mantle wedge beneath the volcanic arc, and (2) high heat flow and thus mantle temperatures throughout the backarc region.

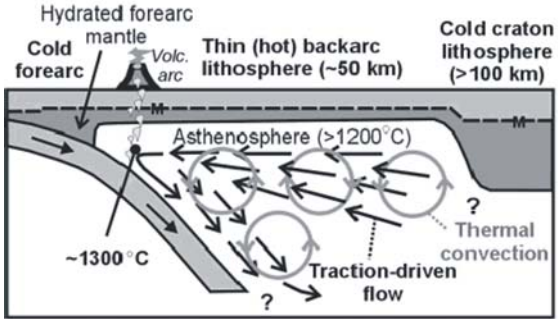

Figure 5. Conceptual model of subduction zone mantle flow. Flow near the volcanic arc is primarily slab-driven.

2.1. 2-D models

Using 2-D finite element models, we investigated the heat budget at the Cascadia subduction zone and examine the thermal consequences of mantle flow induced by traction along the top of the subducting plate [*Currie et al*., 2004]. We propose that slab-driven wedge flow is predominant in the forearc and a region of the back arc near the volcanic front while small-scale free convection in a low-viscosity mantle is necessary to maintain a hot back arc (Figure 5). For traction-driven flow, the thermal structure of the wedge is primarily determined by the mantle rheology and the assumed thermal

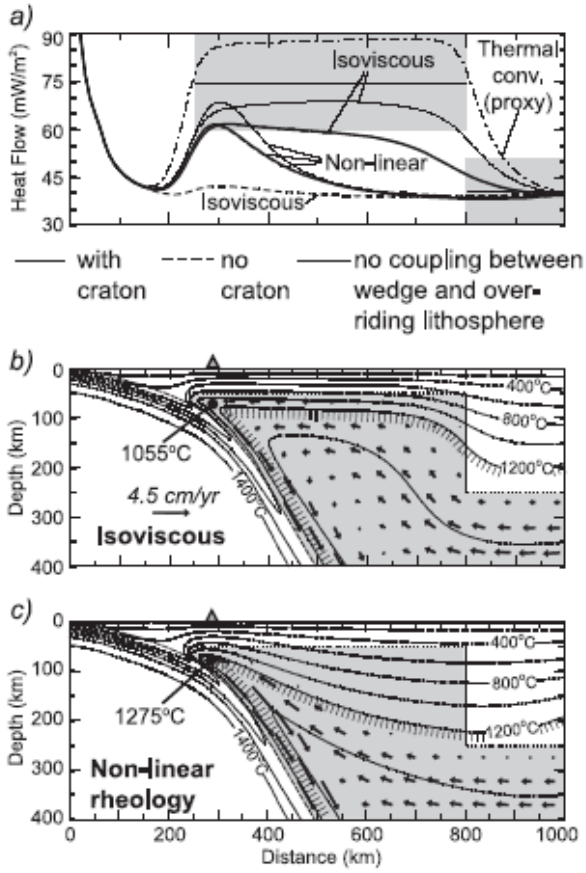

Figure 6. Cascadia thermal models with a rigid 250 km thick craton lithosphere located 800 km from the trench. a) Modelled surface heat flow for models without a craton (dashed), with a craton (solid), and craton models with a free-slip boundary condition between the wedge and over-riding lithosphere (dotted). The dot-dashed line is the heat flow for a proxy model in which the effects of extremely vigourous free convection (Nusselt number of 1000) are simulated. For all models, a cool craton geotherm was prescribed to the landward boundary. b) Thermal model cross-section for an isoviscous wedge. The shaded region indicates where viscous flow was allowed; arrows show flow direction. (c) same as (b), but for a non-linear wedge rheology.

conditions at the landward limit of the backarc. Four boundary conditions for the landward boundary were tested, namely, hot, warm, cold, and craton. The first three of them are illustrated in Figure 7, with two alternative mantle potential temperatures. The "craton" condition is similar to the "cold" condition, except that a rigid body (no flow) representing a hard craton is used as shown in Figure 6. To get high temperatures in the wedge, it is necessary for flow to mine heat from depth. Flow within an isoviscous wedge is too slow to transport a significant amount of heat into the wedge corner (Figure 6). With a more realistic stress- and temperature-dependent wedge rheology, flow is focused into the wedge corner, resulting in rapid flow upward toward the corner and enhanced temperatures below the arc, compatible with temperatures required for arc magma generation (Figure 6). However, this strong flow focusing produces a nearly stagnant region in the shallow backarc mantle, where temperatures and heat flow are much lower than observed. None of the models of simple traction-driven flow were able to simultaneously produce high temperatures beneath the volcanic arc and throughout the backarc. We argue that high temperatures throughout the backarc, particularly in areas that have not undergone extension, provide an important constraint on wedge dynamics. One way to produce hot and isothermal conditions in the backarc is through vigorous small-scale free convection in a low viscosity upper mantle.

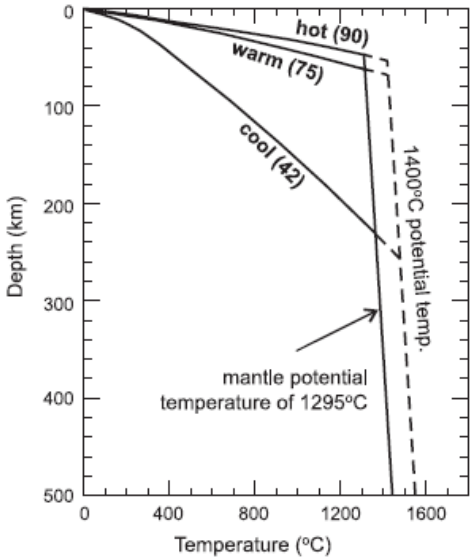

Figure 7. Geotherms prescribed to the landward (backarc) boundary. The numbers in brackets indicate the surface heat flow for each geotherm (mW/m^2). The transition from a conductive gradient to an adiabatic gradient (0.3 ºC/km) is determined by the mantle potential (zero pressure) temperature of 1295 ºC (solid lines) or 1400 ºC (dashed lines).

2.2. 3-D models

In 3-D models, we focus on the effect of slab driven wedge flow near the volcanic arc and investigate effects of along-strike variations in the age and dip of the slab and oblique subduction. 27-node bi-quadratic elements are used for the velocity and temperature fields, and 8-node bi-linear elements are used for the pressure field. We have developed a 3-D code for a massively parallel computing environment.

The construction of the 3-D model follows the same logic as the 2-D models, with two important differences: (1) The 3-D geometry of the slab as constrained by seismic tomography and other studies is incorporated, and (2) the along-strike variation of the age of the incoming Juan de Fuca plate thus heat flow is incorporated. Various models have

been developed. For the following two examples, we use the “warm” condition shown in Figure 7 for the landward boundary. The position of this model boundary for the finite element mesh is much farther away from the trench than shown in the following figures.

The first example is for a Newtonian mantle rheology (Figure 8). The bulge geometry of the subducting slab in the Puget Sound area has a dramatic effect on the thermal structure of the subduction zone. What is the most interesting is that region of slab bulge is colder than what would be expected of a more shallowly dipping slab and by a cross-sectional 2-D model. This is seen in both the surface heat flow (Figure 8a) and mantle wedge corner temperatures (Figure 8c). Note that the colder wedge corner in this place is not a boundary effect, since the actual landward model boundary used in modeling is actually very far from what is shown here for display. This is associated with the mantle wedge flow pattern as affected by the slab geometry. Mantle material tends to flow into the bulge area laterally along strike, resulting in less “mining” of heat from greater depths.

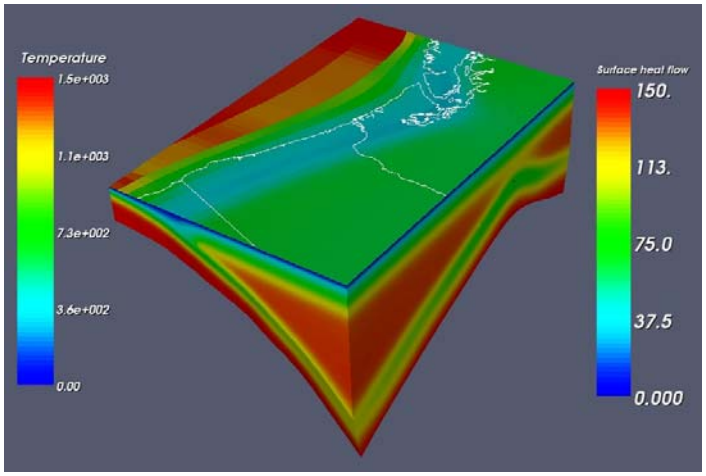

Figure 8a. 3-D thermal model with Newtonian mantle flow. Coastline and state boundaries are shown at the surface for location, length scale, and orientation reference. Surface heat flow is shown on the upper surface of the model. The two vertical surfaces shown temperature distributions.

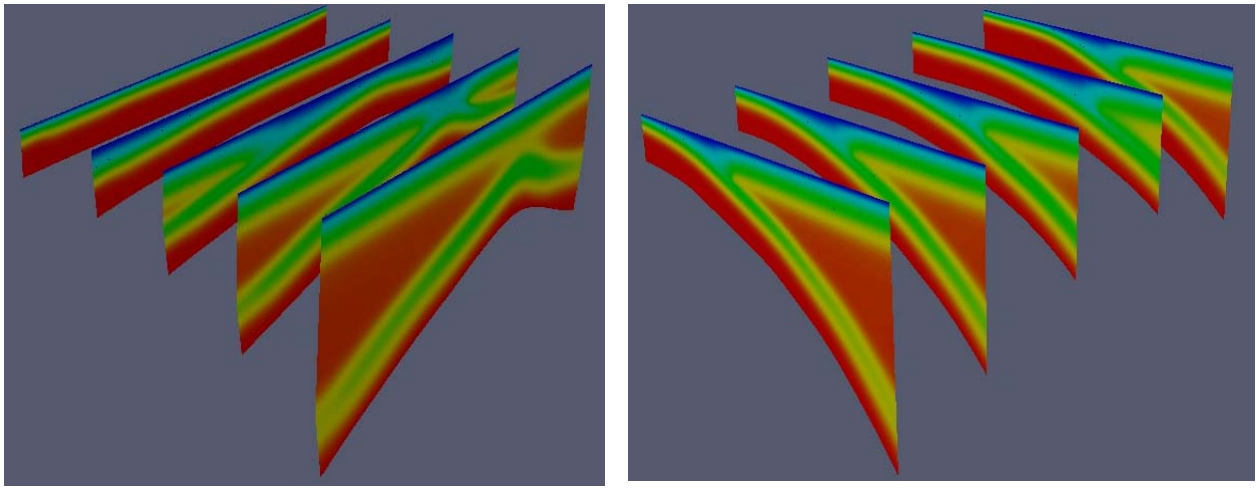

Figure 8b. Strike and dip cross-sections of the model shown in Figure 8a. Color scale for temperature is the same as in Figure 8a.

The next example is for the temperature and stress dependent power-law mantle rheology (dislocation creep) (Figure 9). As in 2-D models with the same rheology, the 3-D model shows channeling of flow from deeper mantle into the mantle wedge corner, causing much higher temperature in the corner than does the Newtonian model. Because the nonlinear rheology and hence much rapid spatial change in flow rate, changes from lower and higher temperatures occur much faster in the Newtonian model (temperature plots appear to be “sharper”). However, similar to the Newtonian model, the slab bulge results in lower temperature and heat flow in the Pudget Sound region than what would be predicted by 2-D models. The model results are yet to be further explored by comparison with heat flow observations and seismicity. Similar 3-D thermal models are being developed for the Nankai subduction zone, where slab geometry changes more drastically along strike.

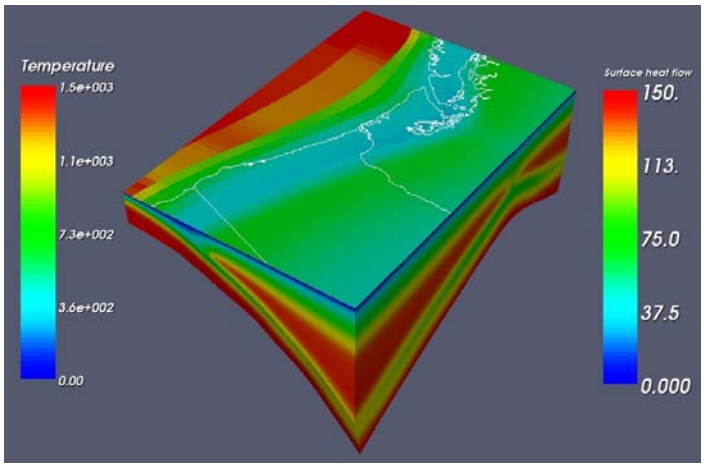

Figure 9a. 3-D thermal model with power-law mantle flow. Coastline and state boundaries are shown at the surface for location, length scale, and orientation reference. Surface heat flow is shown on the upper surface of the model. The two vertical surfaces shown temperature distributions.

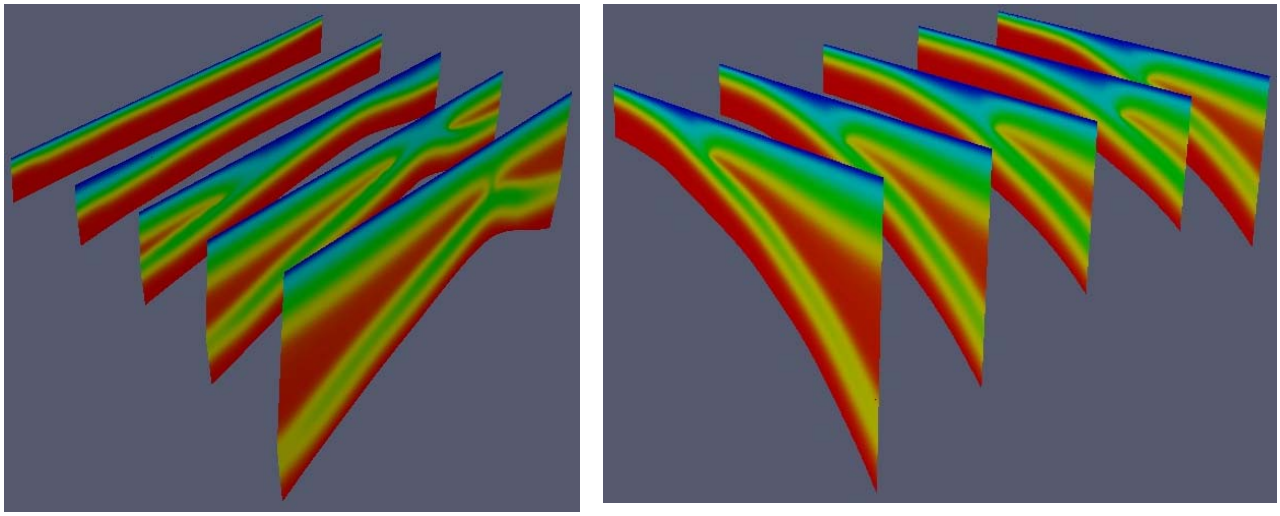

Figure 9b. Strike and dip cross-sections of the model shown in Figure 9a. Color scale for temperature is the same as in Figure 9a.

References (Those marked with * are publications from this study)

Brocher, T. M., T. Parsons, K. C. Creager, R. S. Crosson, N. P. Symons, G. D. Spence, B. C. Zelt, P. T. C. Hammer, R. D. Hyndman, D. C. Mosher, A. M. Tr´ehu, K. C. Miller, R. S. ten Brink, M. A. Fisher, T. L. Pratt, M. G. Alvarez, B. C. Beaudoin, K. E. Louden, and C. S. Weaver (1999), Wide–angle seismic recordings from the 1998 Seismic Hazards Investigation Of Puget Sound (SHIPS), Western Washington and British Colombia, *USGS Open-File Report 99–314*.

Brocher, T. M., T. Parsons, A. M. Tr´ehu, C. M. Snelson, and M. A. Fisher (2003), Seismic evidence for widespread serpentinized forearc upper mantle along the Cascadia margin, *Geology*, *31*, 267–270.

Cassidy, J. F. and R. M. Ellis (1993), S-wave velocity structure of the northern Cascadia subduction zone, *J. Geophys. Res. 98*, 4407–4421.

Cassidy J. F., and F.Waldhauser (2003), Evidence for both crustal and mantle earthquakes in the subducting Juan de Fuca plate, *Geophys. Res. Lett.*, *30*, 1095, doi:10.1029/2002GL015511.

*Currie, C. A., K. Wang, R.D. Hyndman, and J. He (2004), The thermal effects of slab-driven mantle flow above a subducting plate: The Cascadia subduction zone, submitted to *Earth Planet. Sci. Lett.*, *223*, 35-48.

Fisher, M. A., et al. (1999), Seismic survey probes urban earthquake hazards in Pacific Northwest, *Eos, Trans. AGU, 80(2)*, 13–17.

Hacker B. R., S. M. Peacock, G. A. Abers, and S. D. Holloway (2003), Subduction factory 2. Are intermediate-depth earthquakes in subducting slabs linked to metamorphic dehydration reactions?, *J. Geophys. Res.*, *108* , 2030, doi:10.1029/2001JB001129.

Kirby, S.H., E.R., Engdahl, and R., Denlinger (1996), Intraslab earthquakes and arc volcanism: Dual physical expressions of crustal and uppermost mantle metamorphism in subducting slabs, in *Subduction: Top to bottom*, *Edited by* G.E. Bebout, D.W. Scholl, S.H. Kirby, and J.P. Platt, American Geophysical Union, Geophysical Monograph, *96*, 195-214.

Miller, K. C., G. R. Keller, J. M. Gridley, J. H. Luetgert, W. D. Mooney, and H. Thybo (1997), Crustal structure along the west flank of the Cascades, western Washington, *J. Geophys. Res.*, *102*, 17857–17873.

Mooney, W. D. and R. Meissner (1991), Continental crustal evolution observations, *Eos Trans. AGU*, *72*, 537–541.

Peacock, S. M., and K. Wang (1999), Seismic consequences of warm versus cool subduction metamorphism: Examples from Southwest and Northeast Japan, *Science*, *286*, 937-939.

Peacock, S. M., K. Wang, and A. M. McMahon (2002), Thermal structure and metamorphism of subducting oceanic crust: Insight into Cascadia inslab earthquakes, *In* The Cascadia Subduction Zone And Related Subduction Systems - Seismic Structure, Intraslab Earthquakes and Processes, and Earthquake Hazards, *Edited by* S. Kirby, K. Wang and S. Dunlop, *USGS Open-File Report 02328*, 123–126.

*Ramachandran, K., S. E. Dosso, G. D. Spence, R. D. Hyndman, T. M. Brocher (2005a), Forearc Structure Beneath Southwestern British Columbia: A 3-D Tomographic Velocity Model, *J. Geophys. Res.*, 110, doi:10.1029/2004JB003258.

*Ramachandran, K., R. D. Hyndman, and T. M. Brocher (2005b), Northern Cascadia subduction zone: Tomographic 3D P-wave velocity structure, *Geophys. J. Int*., in press.

*Wada, I., K.Wang, and Y. Ishikawa (2004), Stress and Metamorphic Conditions forWarm-slab Earthquakes: Geiyo Area, Southwest Japan, *Eos Trans. AGU, 85(17)*, Jt. Assem. Suppl., Abstract S32A-06.

*Wang, K., J. F. Cassidy, I. Wada, and A. J. Smith, Effects of metamorphic crustal densification on earthquake size in warm slabs, *Geophys. Res. Lett., 31*, L01605, doi:10.1029/2003GL018644, 2004a.

*Wang, K., I. Wada, and Y. Ishikawa, Qualitative analyses of stresses in the subducting slab beneath Southwest Japan, *J. Geophys. Res*., *109*, B08304, doi:10.1029/2003JB002888, 2004b.